

Remote effects spatial process models for modeling teleconnections

Joshua Hewitt¹, Jennifer A. Hoeting¹, James M. Done² and Erin Towler²

¹Colorado State University

²National Center for Atmospheric Research

Abstract: While most spatial data can be modeled with the assumption that distant points are uncorrelated, some problems require dependence at both far and short distances. We introduce a model to directly incorporate dependence in phenomena that influence a distant response. Spatial climate problems often have such modeling needs as data are influenced by local factors in addition to remote phenomena, known as teleconnections. Teleconnections arise from complex interactions between the atmosphere and ocean, of which the El Niño–Southern Oscillation teleconnection is a well-known example. Our model extends the standard geostatistical modeling framework to account for effects of covariates observed on a spatially remote domain. We frame our model as an extension of spatially varying coefficient models. Connections to existing methods are highlighted and further modeling needs are addressed by additionally drawing on spatial basis functions and predictive processes. Notably, our approach allows users to model teleconnected data without pre-specifying teleconnection indices, which other methods often require. We adopt a hierarchical Bayesian framework to conduct inference and make predictions. The method is demonstrated by predicting precipitation in Colorado while accounting for local factors and teleconnection effects with Pacific Ocean sea surface temperatures. We show how the proposed model improves upon standard methods for estimating teleconnection effects and discuss its utility for climate applications.

Keywords: Spatial basis functions, Hierarchical, Bayesian, Climate, Empirical orthogonal functions

1 Introduction

While most spatial data can be modeled with the assumption that distant points are uncorrelated, some problems require dependence at both far and short distances. Spatial climate data is an example of the latter, as it is influenced by local (i.e., short distance) factors, as well as by remote (i.e., far distance) phenomena called teleconnections. Teleconnections refer to changes in patterns of large-scale atmospheric circulation that can drive changes in temperature and precipitation in distant regions (e.g., [Tsonis & Swanson, 2008](#); [Ward et al., 2014](#)). Most teleconnection modeling approaches in the statistical literature do not explicitly estimate dependence within remote phenomena. The statistical literature includes spatially varying coefficient models, analogs, and covariance matrix estimation ([Calder, Craigmire, & Mosley-Thompson, 2008](#); [Choi, Li, Zhang, & Li, 2015](#); [McDermott & Wikle, 2016](#); [Wikle & Anderson, 2003](#)). Explicitly modeling dependence in remote phenomena can add physically sensible structure that improves prediction accuracy and addresses some modeling challenges. We propose a geostatistical model that addresses this unmet modeling need for teleconnection.

Teleconnections can be forced by changes in sea surface temperature (SST), and there have been many observational and modeling studies studying the link between SSTs, circulation patterns, and impacts on global and regional climate. Several seminal studies connect U.S. precipitation with SST anomalies in the tropical Pacific due to the El Niño–Southern Oscillation teleconnection (ENSO) ([Montroy, 1997](#); [Montroy, Richman, & Lamb, 1998](#)), as well as with SST anomalies in the Pacific (e.g., [Dong & Dai, 2015](#)). The ENSO teleconnection has been critical in seasonal climate forecasting ([Goddard et al., 2001](#)), and decadal variability of sea surface temperature anomalies have been identified as a source of potential

skill for decadal predictions that look out one year to a decade (Meehl et al., 2009). In terms of the latter, decadal predictions produced from global climate models (GCMs) have shown skill in reproducing ocean and land temperatures, and less skill in precipitation (Meehl et al., 2014). This is the general finding for GCMs: while GCMs perform poorly in predicting precipitation directly, they can skillfully reproduce surface temperatures and large-scale patterns (Flato et al., 2013). Direct precipitation prediction by GCMs is challenging because of complex and interacting multi-scale physical precipitation processes, resulting in large uncertainty in future precipitation patterns (Deser, Phillips, Bourdette, & Teng, 2012). As such, this provides a motivating example for demonstrating a teleconnection model that can be used in conjunction with GCM output to estimate impacts on precipitation.

Developing a teleconnection model for application with GCM output has overlaps with the burgeoning field of statistical downscaling. Statistical downscaling methods use large-scale variables to draw inference on regional variables. Similar to what is being proposed here, a type of statistical downscaling called perfect prognosis downscaling (Maraun et al., 2010) develops a statistical relationship between observed large-scale predictors and local-scale weather phenomena (e.g., Bruyere, Holland, & Towler, 2012; Towler, PaiMazumder, & Holland, 2016; Wilby et al., 1998). Common models used for perfect prognosis downscaling do not explicitly model spatial dependence. Maraun et al. (2010) review methods used in the climate literature, which include linear models, analogs, and machine learning techniques like neural networks. Dependence is often indirectly modeled by using principle component or canonical correlation basis functions as predictors and applying various corrections to uncertainties (cf. Karl, Wang, Schlesinger, Knight, & Portman, 1990). After statistical relationships are developed and validated on observed datasets, models can be applied to large-scale GCM output to obtain an estimate of the desired predictant. Clearly, perfect prognosis methods are highly dependent on the selected predictors and model (Fowler, Blenkinsop, & Tebaldi, 2007).

We propose a remote effects spatial process (RESP) model that extends spatially varying

coefficient models to directly model dependence in remote phenomena and address several modeling challenges. Spatially modeling dependence in remote phenomena adds sensible structure to teleconnection models which, in turn, allows better use of the data than standard models. Standard spatially varying coefficient models regress a local response $Y(\mathbf{s}, t)$ with spatio-temporal error $w(\mathbf{s}, t)$ onto local covariates $\mathbf{x}(\mathbf{s}, t)$ through

$$(1) \quad Y(\mathbf{s}, t) = \mathbf{x}(\mathbf{s}, t)^T \boldsymbol{\beta} + \mathbf{z}(t)^T \boldsymbol{\theta}(\mathbf{s}) + w(\mathbf{s}, t)$$

which includes adjustment for spatially-varying effects $\boldsymbol{\theta}(\mathbf{s}) \in \mathbb{R}^k$ associated with a second vector $\mathbf{z}(t) \in \mathbb{R}^k$ of k covariates (Banerjee, Carlin, & Gelfand, 2015, Section 9.6.2). As applied to teleconnection, the covariate vector $\mathbf{z}(t)$ contains one or more indices that quantify the overall strength or state of large-scale patterns, like ENSO or the North Atlantic Oscillation (Calder et al., 2008; Wikle & Anderson, 2003). While effective, the model (1) assumes relevant large-scale patterns are known a priori (e.g., ENSO). However, relevant teleconnection indices can depend on the study region and thus be unknown at the start of an analysis (Towler et al., 2016). The spatially varying coefficient model (1) will be inefficient if driven by poorly chosen teleconnection indices. Standard formulations of (1) also model within-site covariances for spatially varying effects $\Lambda = \text{Cov}(\boldsymbol{\theta}(\mathbf{s})) \in \mathbb{R}^{k \times k}$ with non-spatial covariance matrices. While the issue may be less important for orthogonal teleconnection indices, typical indices are defined with respect to different covariates and zonal averages so may not be orthogonal (cf. Ashok, Behera, Rao, Weng, & Yamagata, 2007; Mantua, Hare, Zhang, Wallace, & Francis, 1997). Instead, teleconnection indices may have spatial structure induced by remote covariates. The RESP model introduced below directly incorporates remote covariates instead of using teleconnection indices and can offer potential improvement for the a priori and spatial structure concerns (Section 2.1). Notably, the RESP model does not lose generality since direct connections can be drawn to standard spatially varying coefficient models (Section 2.3).

More generally, the RESP model represents a less-common class of spatial analysis problems that provide rich opportunities for study. We introduce our teleconnection model in the general context of a spatial regression problem involving local and spatially remote covariates (Section 2.1). The local and spatially remote covariates are allowed to have different spatial correlations structures reflecting their different relationships with the response. Figure 1 schematically illustrates the general teleconnection problem in which local $\mathbf{x}(\mathbf{s}, t)$ and remote $z(\mathbf{r}, t)$ covariates impact a local spatio-temporal response $Y(\mathbf{s}, t)$. The RESP model accounts for the influence of covariates observed on a geographically remote domain $z(\mathbf{r}, t)$.

We demonstrate the capacity of the RESP model by validating its ability to predict Colorado winter precipitation in a cross-validation study (Section 3). Our study represents a type of perfect prognosis problem in which future precipitation will be studied with covariates that have been simulated by GCMs. Since atmospheric processes have relatively short memory, it is reasonable to assume winter precipitation is conditionally independent across years when local and remote covariates are given. Therefore, we develop the RESP model assuming there is no meaningful temporal dependence. We conclude with discussions of temporal extensions and other directions for future work and further application (Section 4).

2 A geostatistical model for spatially remote covariates

Teleconnection manifests as an aggregate property of spatially continuous covariates. For example, consider the sea surface temperature (SST) at location \mathbf{r} and time t , $z(\mathbf{r}, t)$. In spatially varying coefficient models (1), it is common to adopt a teleconnection index $z(t) \in \mathbb{R}$ that is defined as the average SST $z(\mathbf{r}, t)$ over a region $\mathcal{R} \subset \mathcal{D}_Z$. In (1), the spatially varying coefficient term $z(t)\theta(\mathbf{s})$ motivates the RESP model through the expansion

$$(2) \quad z(t)\theta(\mathbf{s}) = \frac{1}{|\mathcal{R}|} \int_{\mathcal{R}} z(\mathbf{r}, t)\theta(\mathbf{s}) d\mathbf{r}.$$

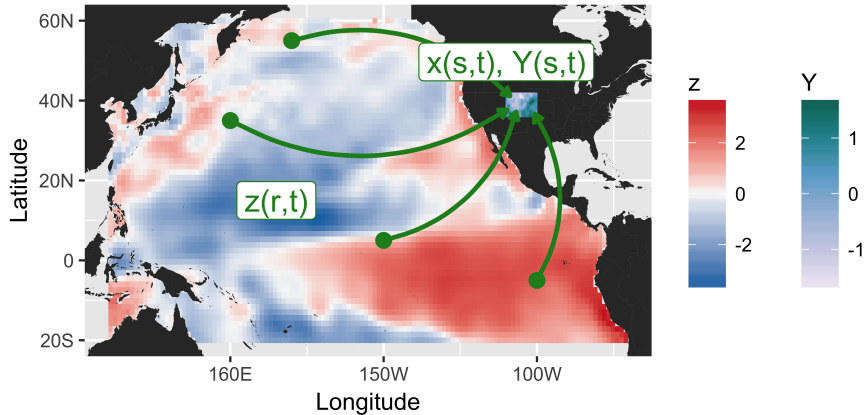


Figure 1: Schematic illustration of a teleconnection problem. Colorado precipitation $Y(\mathbf{s}, t)$ is influenced by both local covariates $\mathbf{x}(\mathbf{s}, t)$ and remote covariates $z(\mathbf{r}, t)$. The remote covariates shown here are standardized anomalies of average monthly Pacific Ocean sea surface temperatures during Winter, 1982. The data come from the ERA-Interim reanalysis dataset (Dee et al., 2011).

The RESP model extends the integral in (2) to the entire remote domain \mathcal{D}_Z and allows $\theta(\mathbf{s})$ to vary with respect to \mathbf{r} , distinguishing it from spatially varying coefficient models (Section 2.1). Integration is a natural construct for aggregating effects of spatially continuous covariates, represents the conceptual limit of studying teleconnection with increasingly fine subsets of \mathcal{R} , and allows study of teleconnection with additional spatial structure and without defining indices a priori.

2.1 Model formulation

The remote effects spatial process (RESP) model extends the standard geostatistical setting in which a local response variable $Y(\mathbf{s}, t) \in \mathbb{R}$ and known covariate vector $\mathbf{x}(\mathbf{s}, t) \in \mathbb{R}^p$ are observable at discrete time points $t \in \mathcal{T} = \{t_1, \dots, t_{n_t}\}$ and at locations \mathbf{s} in a continuous domain \mathcal{D}_Y . The RESP model includes the effects of known remote covariates $z(\mathbf{r}, t) \in \mathbb{R}$, which are observable at locations \mathbf{r} in a continuous domain that is spatially disjoint from

the local response—i.e., in a continuous \mathcal{D}_Z s.t. $\mathcal{D}_Y \cap \mathcal{D}_Z = \emptyset$. The RESP model is given by

$$(3) \quad Y(\mathbf{s}, t) = \mathbf{x}^T(\mathbf{s}, t)\boldsymbol{\beta} + w(\mathbf{s}, t) + \varepsilon(\mathbf{s}, t) + \gamma(\mathbf{s}, t)$$

where the regression coefficients $\boldsymbol{\beta} \in \mathbb{R}^p$, spatially correlated noise $w(\mathbf{s}, t)$, and independent noise $\varepsilon(\mathbf{s}, t)$ are standard components for spatial regression models (Banerjee et al., 2015, Chapters 6, 9, 11). In the RESP model the teleconnection effect given by $\gamma(\mathbf{s}, t)$ is defined by

$$(4) \quad \gamma(\mathbf{s}, t) = \int_{\mathcal{D}_Z} z(\mathbf{r}, t) \alpha(\mathbf{s}, \mathbf{r}) d\mathbf{r}$$

which describes the net effect of the remote covariates $z(\mathbf{r}, t)$ on the continuous spatial process $Y(\mathbf{s}, t)$ at discrete time t . The integral (4) reduces to a sum for finite samples, in which the remote covariates $z(\mathbf{r}, t)$ are observed at $n_r < \infty$ locations. Multivariate extensions of (4) are discussed in Section 4.

The remote (or teleconnection) coefficients $\alpha(\mathbf{s}, \mathbf{r})$ are spatially correlated and doubly-indexed by $(\mathbf{s}, \mathbf{r}) \in \mathcal{D}_Y \times \mathcal{D}_Z$. The spatial correlation and double-indexing of $\alpha(\mathbf{s}, \mathbf{r})$ represents teleconnection effects that vary regionally in the sense that the response $Y(\mathbf{s}, t)$ at one location $\mathbf{s} \in \mathcal{D}_Y$ can respond to the remote covariates $z(\mathbf{r}, t)$ more strongly than the response $Y(\mathbf{s}', t)$ at another location $\mathbf{s}' \in \mathcal{D}_Y$. Similarly, the response $Y(\mathbf{s}, t)$ at one location $\mathbf{s} \in \mathcal{D}_Y$ can respond differently to remote covariates $z(\mathbf{r}, t)$ and $z(\mathbf{r}', t)$ at distinct remote locations $\mathbf{r}, \mathbf{r}' \in \mathcal{D}_Z$. Thus, the remote coefficients $\alpha(\mathbf{s}, \mathbf{r})$ vary spatially and use the remote covariates $z(\mathbf{r}, t)$ to provide local adjustment to the mean response. The teleconnection term $\gamma(\mathbf{s}, t)$ is well defined because we assume the remote covariates $z(\mathbf{r}, t)$ are known and square-integrable over \mathcal{D}_Z at each time point t (Adler & Taylor, 2007, Section 5.2).

The RESP model provides a simple geostatistical approach to modeling teleconnections by extending spatial regression models to incorporate data from spatially remote regions. The teleconnection term $\gamma(\mathbf{s}, t)$ distinguishes the RESP model (3) from standard geostatis-

tical models, in which—for example—the responses $Y(\mathbf{s}, t)$ and $Y(\mathbf{s}', t)$ at distinct spatial locations $\mathbf{s}, \mathbf{s}' \in \mathcal{D}_Y$ are only influenced by distinct covariates $x(\mathbf{s}, t)$ and $x(\mathbf{s}', t)$. To model the influence of teleconnection phenomena the RESP model lets the remote covariates $z(\mathbf{r}, t)$ simultaneously influence the responses $Y(\mathbf{s}, t)$ and $Y(\mathbf{s}', t)$.

Geostatistical modeling conventions use mean zero Gaussian processes to specify the randomness of the unknown, spatially correlated components $w(\mathbf{s}, t)$ and $\alpha(\mathbf{s}, \mathbf{r})$, and an independent processes to specify the noise $\varepsilon(\mathbf{s}, t)$ —the nugget. We complete the Gaussian process specifications by defining the covariance functions for the spatially correlated components. Let C_w and C_α respectively be the covariance functions for $w(\mathbf{s}, t) + \varepsilon(\mathbf{s}, t)$ and $\alpha(\mathbf{s}, \mathbf{r})$, where

$$(5) \quad C_w \{(\mathbf{s}, t), (\mathbf{s}', t')\} = (\kappa(\mathbf{s}, \mathbf{s}'; \boldsymbol{\theta}_w) + \sigma_\varepsilon^2 \mathbb{1}(\mathbf{s} = \mathbf{s}')) \mathbb{1}(t = t'),$$

$$(6) \quad C_\alpha \{(\mathbf{s}, \mathbf{r}), (\mathbf{s}', \mathbf{r}')\} = (\kappa(\mathbf{s}, \mathbf{s}'; \boldsymbol{\theta}_w) + \sigma_\varepsilon^2 \mathbb{1}(\mathbf{s} = \mathbf{s}')) \kappa(\mathbf{r}, \mathbf{r}'; \boldsymbol{\theta}_\alpha).$$

Our model may be developed with any spatial covariance function κ , but here we choose to work with the stationary Matérn covariance

$$(7) \quad \kappa(\mathbf{u}, \mathbf{v}; \boldsymbol{\theta}) = \frac{\sigma^2}{2^{\nu-1} \Gamma(\nu)} (d(\mathbf{u}, \mathbf{v}) / \rho)^\nu K_\nu(d(\mathbf{u}, \mathbf{v}) / \rho)$$

for spatial locations \mathbf{u} and \mathbf{v} , and parameter vector $\boldsymbol{\theta} = (\sigma^2, \rho, \nu)^T$. The function $d(\mathbf{u}, \mathbf{v})$ must be an appropriate distance function (e.g., great-circle distances for locations on a sphere), $\sigma^2 > 0$ is a scaling parameter, $\nu > 0$ is a smoothness parameter, $\rho > 0$ is a range parameter, and K_ν is the modified Bessel function of the second kind with order ν . In covariance function definitions (5) and (6), $\mathbb{1}$ represents the indicator function and σ_ε^2 represents the variance of the nugget process which we specify to be a collection of independent and identically distributed mean zero Gaussian random variables—i.e., $\varepsilon(\mathbf{s}, t) \stackrel{iid}{\sim} \mathcal{N}(0, \sigma_\varepsilon^2) \forall (\mathbf{s}, t) \in \mathcal{D}_Y \times \mathcal{T}$.

While the definitions (5) and (6) for the local and remote covariances C_w and C_α can

be generalized, the definitions restrict our use of the RESP model to working in the perfect prognosis downscaling setting described at the end of Section 1. The responses $Y(\mathbf{s}, t)$ and $Y(\mathbf{s}, t')$ for $t \neq t'$ are independent given covariates and sufficiently separated time points, like successive winters (e.g., winter 1991, winter 1992, etc.). The remote covariates in the teleconnection term (4) naturally induce temporal non-stationarity in the response's variance; extensions to accommodate serial dependence are discussed in Section 4. The remote covariance C_α also induces a separable structure for the remote coefficients $\alpha(\mathbf{s}, \mathbf{r})$, which constrains the spatial variability of teleconnection effect fields and simultaneously constrains the teleconnection effects $\{\alpha(\mathbf{s}, \mathbf{r}) : \mathbf{r} \in \mathcal{D}_Z\}$ and $\{\alpha(\mathbf{s}', \mathbf{r}) : \mathbf{r} \in \mathcal{D}_Z\}$ to be similar for nearby locations $\mathbf{s}, \mathbf{s}' \in \mathcal{D}_Y$. Simpler covariance structures for the teleconnection effects $\alpha(\mathbf{s}, \mathbf{r})$ may not capture these physical properties of teleconnection as directly. Similarly, although climate data are often available as gridded data products, we choose to work with geostatistical covariance models (or their discrete approximations, e.g., Lindgren, Rue, & Lindström, 2011) instead of neighborhood-based spatial models so that we may avoid inducing potentially counterintuitive covariance structures (Assunção & Krainski, 2009; Wall, 2004).

2.2 Reduced rank approximation

To apply the RESP model (3), additional constraints need to be imposed due to the potential multicollinearity in the covariates. Remote covariates $z(\mathbf{r}, t)$ in teleconnection applications will often consist of data that measure ocean properties at high spatial resolution, like sea surface temperature or sea level pressure. This raises concerns for estimating the remote coefficients $\alpha(\mathbf{s}, \mathbf{r})$ in (4) as the main trends in the remote covariates $z(\mathbf{r}, t)$ are highly collinear over \mathcal{D}_Z . Physically, however, this suggests the remote coefficients should be highly correlated as well. We use predictive processes to mitigate multicollinearity in the remote covariates, which is an alternative motivation for predictive processes. Banerjee, Gelfand, Finley, and Sang (2008) originally introduce predictive processes so that parameters of geo-

statistical models can be estimated for large spatial datasets, rather than as an approach for mitigating spatial multicollinearity. We consider more general basis expansions of remote coefficients in Section 2.3.

We assume the remote coefficients $\alpha(\mathbf{s}, \mathbf{r})$ can be well represented by weighted averages of remote coefficients $\alpha(\mathbf{s}, \mathbf{r}^*)$ at knot locations $\mathbf{r}_1^*, \dots, \mathbf{r}_k^* \in \mathcal{D}_Z$, so we make the simplifying approximation that, for some weight function $h(\mathbf{r}, \mathbf{r}')$ and associated vector $\mathbf{h}^*(\mathbf{r}) = [h(\mathbf{r}, \mathbf{r}_j^*)]_{j=1}^k \in \mathbb{R}^k$, we can write

$$(8) \quad \alpha(\mathbf{s}, \mathbf{r}) = \sum_{j=1}^k h(\mathbf{r}, \mathbf{r}_j^*) \alpha(\mathbf{s}, \mathbf{r}_j^*) = \mathbf{h}^*(\mathbf{r})^T \boldsymbol{\alpha}^*(\mathbf{s}),$$

where $\boldsymbol{\alpha}^*(\mathbf{s}) = [\alpha(\mathbf{s}, \mathbf{r}_j^*)]_{j=1}^k \in \mathbb{R}^k$. The predictive process approach uses kriging to motivate a choice for the weight vector $\mathbf{h}^*(\mathbf{r})$, which induces a weight function h . Using Gaussian processes in Section 2.1 to model the remote coefficients implies that $\alpha(\mathbf{s}, \mathbf{r})$ and $\boldsymbol{\alpha}^*(\mathbf{s})$ are jointly normally distributed, yielding the conditional expectation for $\alpha(\mathbf{s}, \mathbf{r})$

$$(9) \quad E[\alpha(\mathbf{s}, \mathbf{r}) | \boldsymbol{\alpha}^*(\mathbf{s})] = \mathbf{c}^*(\mathbf{r})^T R^{*-1} \boldsymbol{\alpha}^*(\mathbf{s})$$

in which $\mathbf{c}^*(\mathbf{r}) = [C_\alpha\{(\mathbf{s}, \mathbf{r}), (\mathbf{s}, \mathbf{r}_j^*)\}]_{j=1}^k \in \mathbb{R}^k$ and $R^* \in \mathbb{R}^{k \times k}$ with entries $R_{ij}^* = C_\alpha\{(\mathbf{s}, \mathbf{r}_i^*), (\mathbf{s}, \mathbf{r}_j^*)\}$. Note that the assumption in (6) that C_α is stationary means that $\mathbf{c}^*(\mathbf{r})$ and R^* do not depend on \mathbf{s} , despite the term appearing in their definitions. The predictive process approach uses the conditional expectation (9) to define the weight vector $\mathbf{h}^*(\mathbf{r}) = R^{*-1} \mathbf{c}^*(\mathbf{r})$ in the approximation (8). Banerjee et al. (2008) show that these types of approximations are reduced rank projections that can capture large-scale spatial structures in data.

Beyond mitigating the statistical issue of multicollinearity, the predictive process approach relates the RESP model to spatially varying coefficient models (1) and also has a scientific interpretation for teleconnection. Using the reduced rank approximation (8) to

manipulate the integral in (3) shows that the reduced rank approximation can be interpreted as inducing transformed covariates $z^*(\mathbf{r}^*, t)$ via

$$\begin{aligned}
 \int_{\mathcal{D}_Z} z(\mathbf{r}, t) \alpha(\mathbf{s}, \mathbf{r}) d\mathbf{r} &= \int_{\mathcal{D}_Z} z(\mathbf{r}, t) \sum_{j=1}^k h(\mathbf{r}, \mathbf{r}_j^*) \alpha(\mathbf{s}, \mathbf{r}_j^*) d\mathbf{r} \\
 (10) \qquad \qquad \qquad &= \sum_{j=1}^k \alpha(\mathbf{s}, \mathbf{r}_j^*) z^*(\mathbf{r}_j^*, t)
 \end{aligned}$$

where $z^*(\mathbf{r}_j^*, t) = \int_{\mathcal{D}_Z} z(\mathbf{r}, t) h(\mathbf{r}, \mathbf{r}_j^*) d\mathbf{r}$. The $z^*(\mathbf{r}_j^*, t)$ and $\alpha(\mathbf{s}, \mathbf{r}_j^*)$ may be collected into the covariate vector $\mathbf{z}(t)$ and spatially varying effects $\boldsymbol{\theta}(\mathbf{s})$ in (1). We remark that the RESP model differs from standard spatially varying coefficient models in that the $z^*(\mathbf{r}_j^*, t)$ represent induced—rather than a priori—covariates, and the $\alpha(\mathbf{s}, \mathbf{r}_j^*)$ inherit spatial structure from the model’s formulation.

Scientifically, the predictive process approach to addressing multicollinearity in the remote covariates reduces the remote covariates $z(\mathbf{r}, t)$, $\mathbf{r} \in \mathcal{D}_Z$ at each time point to k spatially-averaged indices $z^*(\mathbf{r}^*, t)$ centered at \mathbf{r}^* for $\mathbf{r}^* \in \{\mathbf{r}_1^*, \dots, \mathbf{r}_k^*\}$. This manipulation is fairly generic and should be applicable to all predictive process models. For teleconnection, this manipulation connects the RESP model to one set of standard teleconnection methodologies in which teleconnection effects are measured with respect to ocean indices based on spatial averages of remote covariates (Ashok et al., 2007; Towler et al., 2016).

2.3 Spatial basis function transformation of remote coefficients

The RESP model (3) is also related to another set of standard teleconnection methodologies in which teleconnection effects are measured with respect to complex ocean indices such as empirical orthogonal functions (Montroy, 1997; Ting & Wang, 1997). Spatial basis functions provide a means to reparameterize the RESP model and show it can identify and leverage known teleconnections with complex patterns. We use the following reparameterization of the teleconnection effects $\alpha(\mathbf{s}, \mathbf{r})$ to discuss teleconnection between Pacific Ocean sea surface

temperature and Colorado precipitation in Section 3.

Complex teleconnection patterns are often based on spatial basis function expansions of the remote covariates $z(\mathbf{r}, t)$. If there exist weights $\{a_l(t) : l = 1, \dots, K; t \in \mathcal{T}\}$ such that the remote covariates $z(\mathbf{r}, t)$ can be written as a linear combination of continuous, time-invariant basis functions $\{\psi_l(\mathbf{r}) : l = 1, \dots, K; \mathbf{r} \in \mathcal{D}_Z\}$ via

$$(11) \quad z(\mathbf{r}, t) = \sum_{l=1}^K a_l(t) \psi_l(\mathbf{r}),$$

then linearity of the integral in (4) and reduced rank approximation (8) can induce a reparameterized, reduced-rank teleconnection effect process $\alpha'(\mathbf{s}, l)$ for patterns $l = 1, \dots, K$ by

$$(12) \quad \alpha'(\mathbf{s}, l) = \sum_{j=1}^k \alpha(\mathbf{s}, \mathbf{r}_j^*) \int_{\mathcal{D}_Z} \psi_l(\mathbf{r}) h(\mathbf{r}, \mathbf{r}_j^*) d\mathbf{r}.$$

Note that the transformation appears naturally because

$$(13) \quad \begin{aligned} \int_{\mathcal{D}_Z} z(\mathbf{r}, t) \alpha(\mathbf{s}, \mathbf{r}) d\mathbf{r} &= \int_{\mathcal{D}_Z} \sum_{l=1}^K a_l(t) \psi_l(\mathbf{r}) \sum_{j=1}^k h(\mathbf{r}, \mathbf{r}_j^*) \alpha(\mathbf{s}, \mathbf{r}_j^*) d\mathbf{r} \\ &= \sum_{l=1}^K a_l(t) \sum_{j=1}^k \alpha(\mathbf{s}, \mathbf{r}_j^*) \int_{\mathcal{D}_Z} \psi_l(\mathbf{r}) h(\mathbf{r}, \mathbf{r}_j^*) d\mathbf{r} \\ &= \sum_{l=1}^K a_l(t) \alpha'(\mathbf{s}, l). \end{aligned}$$

As with the reduced rank approximation (8), the transformation (13) also relates the RESP model to spatially varying coefficient models (1) and has scientific relevance for teleconnection. The deterministic remote covariate weights $a_l(t)$ and reparameterized remote coefficients $\alpha'(\mathbf{s}, l)$ may be collected into the covariate vector $\mathbf{z}(t)$ and spatially varying effects $\boldsymbol{\theta}(\mathbf{s})$ in (1). While the covariate weights $a_l(t)$ suggest a priori selection of teleconnection indices, the reparameterization may be applied after model estimation. The $\alpha'(\mathbf{s}, l)$ addi-

tionally inherit spatial structure from the model’s formulation. Scientifically, a special case of (11) are principal component decompositions or the closely related truncated Karhunen–Lòeve expansions, which are referred to as empirical orthogonal functions (EOFs) in climate science. EOFs are particularly useful expansions for teleconnection because these transformations meaningfully characterize phenomena that impact global climate (Ashok et al., 2007).

2.4 Inference

While inference for the RESP model (3) can use standard hierarchical Bayesian modeling techniques, the Bayesian framework provides crucial intuition and interpretation for estimates of teleconnection effects (8) and (12). Full description of model priors and computational techniques for inference are discussed in Supplement A ???. The Gaussian process assumption and separable covariance (6) for the vector of teleconnection coefficients $\boldsymbol{\alpha}^*(\mathbf{s})$ with associated covariance matrix R^* defined in Section 2.2 imply the normally-distributed prior $\boldsymbol{\alpha}^*(\mathbf{s})|R^* \sim \mathcal{N}(\mathbf{0}, R^*)$. Gaussian process assumptions for the RESP model’s spatial correlation also imply the likelihood for the vector of responses observed at n_t timepoints $\mathbf{Y}(\mathbf{s}) = [Y(\mathbf{s}, t_1), \dots, Y(\mathbf{s}, t_{n_t})]^T \in \mathbb{R}^{n_t}$ is

$$(14) \quad \mathbf{Y}(\mathbf{s})| \boldsymbol{\alpha}^*(\mathbf{s}), \boldsymbol{\beta}, R^*, \mathbf{c}^*, \sigma_s^2 \sim \mathcal{N}\left(\mathbf{X}(\mathbf{s})\boldsymbol{\beta} + \mathbf{Z}^{*T}\boldsymbol{\alpha}^*(\mathbf{s}), \sigma_s^2 I_{n_t}\right)$$

with $\sigma_s^2 = C_w\{(\mathbf{s}, t), (\mathbf{s}, t)\}$ and matrices of local covariates $\mathbf{X}(\mathbf{s}) = \left[\mathbf{x}(\mathbf{s}, t)^T\right]_{t=t_1}^{t_{n_t}} \in \mathbb{R}^{n_t \times p}$ and reduced-rank remote covariates $\mathbf{Z}^* \in \mathbb{R}^{k \times n_t}$. The matrix \mathbf{Z}^* is comprised of column vectors $\mathbf{z}_t^* = R^{*-1}\mathbf{c}^{*T}\mathbf{z}_t \in \mathbb{R}^k$ built from remote covariate vectors $\mathbf{z}_t = [z(\mathbf{r}_j, t)]_{j=1}^{n_r} \in \mathbb{R}^{n_r}$. Our formulation of the spatial correlation (5) implies the scalar σ_s^2 is constant across time; non-stationary extensions are discussed in Section 4. Standard Bayesian linear regression

results (Banerjee et al., 2015, Example 5.2) yield the posterior distribution

$$(15) \quad \boldsymbol{\alpha}^*(\mathbf{s}) | \mathbf{Y}(\mathbf{s}), \boldsymbol{\beta}, R^*, \mathbf{c}^*, \sigma_s^2 \sim \mathcal{N}(\sigma_s^{-2} \boldsymbol{\Psi} \mathbf{Z}^* (\mathbf{Y}(\mathbf{s}) - \mathbf{X}(\mathbf{s}) \boldsymbol{\beta}), \boldsymbol{\Psi})$$

for

$$\boldsymbol{\Psi} = \left(R^{*-1} + \sigma_s^{-2} \mathbf{Z}^* \mathbf{Z}^{*T} \right)^{-1}.$$

The connection to Bayesian linear regression lends intuition for inference on the remote effects $\boldsymbol{\alpha}^*(\mathbf{s})$. In particular, the connection provides intuition for using the RESP model when some local covariates $\mathbf{x}(\mathbf{s}, t)$ are also teleconnected with remote covariates \mathbf{z}_t . Remote coefficients can be interpreted as residual teleconnection effects in the sense that they model the impact of remote covariates on the response after removing local effects $\mathbf{X}(\mathbf{s}) \boldsymbol{\beta}$. Properties of regressions also imply patterns in maps of posterior means for $\boldsymbol{\alpha}^*(\mathbf{s})$ may resemble patterns in maps that show pointwise correlations $\text{Cor}_t(z^*(\mathbf{r}^*, t), Y(\mathbf{s}, t))$ between remote covariates at \mathbf{r}^* and responses at \mathbf{s} . Similar regression-based interpretations can be derived for the reparameterized teleconnection coefficients (12).

3 Climate application: Colorado winter precipitation

The RESP model (3) is applied here using remote and local covariates to estimate Colorado winter precipitation. Winter precipitation is important to estimate because it strongly influences Colorado's annual water supply. We investigate the utility of our RESP model for this application because there is considerable uncertainty regarding precipitation that is directly predicted by GCMs. Further, the RESP model can be applied without specifying teleconnection indices a priori, as many common approaches require. Let $Y(\mathbf{s}, t)$ denote

average monthly precipitation in winter for location \mathbf{s} and year t via

$$(16) \quad Y(\mathbf{s}, t) = (Y_{Dec}(\mathbf{s}, t) + Y_{Jan}(\mathbf{s}, t) + Y_{Feb}(\mathbf{s}, t)) / 3$$

in which, for example, $Y_{Dec}(\mathbf{s}, t)$ represents the total December precipitation in year t at location \mathbf{s} . The atmosphere's short memory suggests $Y(\mathbf{s}, t)$ is independent from $Y(\mathbf{s}, t')$ for $t \neq t'$, which is confirmed in an exploratory analysis of Colorado precipitation. Winter precipitation is important to estimate at long time scales because it strongly influences Colorado's annual water supply.

We formulate the problem of estimating precipitation as a need to estimate entire precipitation fields when only covariates are available. We build the RESP model (3) with historical data to estimate a statistical relationship between average monthly winter precipitation in Colorado and land and sea surface temperatures. We discuss inference for the RESP model to illustrate that it can estimate teleconnection patterns without specifying teleconnection indices a priori (Section 3.4.1). A leave-one-out cross-validation study validates the model's effectiveness (Section 3.4.2), especially in relation to other common downscaling methods (Section 3.3). Although beyond the scope of this study, a next step for future work would be to apply the RESP model to simulated GCM output.

3.1 Data

The ERA-Interim reanalysis dataset provides reconstructions of historical sea surface temperatures and local covariates (Dee et al., 2011). The response, precipitation, comes from the PRISM dataset (Daly et al., 2008). We limit our study period to 1981 through 2013 because earlier records of large scale climate are less complete. Both datasets are reanalysis products, which are necessary because working directly with observations can be challenging. Raw data may be from various sources and are often spatially sparse and temporally incomplete. Reanalysis products use statistical techniques and physical relationships to reproduce

consistent datasets at regular, gridded locations with complete records after removing or correcting observations that are physically inconsistent or from stations with potential data collection issues.

This study uses data averaged over the boreal winter months (December, January, February) because Northern Hemisphere teleconnections are often strongest in winter (Nigam & Baxter, 2015). We simplify the demonstration using spatially-referenced variables average surface air temperature over Colorado (T) and average Pacific Ocean sea surface temperatures (SST) between 120°E – 70°W and 20°S – 60°N to predict the spatially-referenced response, average winter precipitation in Colorado (P). We standardize all data to remove the impact of orographic and other location-based effects by removing the pointwise mean from all data and scaling data to have unit variance. We additionally scale the SST values by n_r^{-1} to ensure the remote coefficient magnitudes are independent of the resolution at which SST is measured. We standardize our data before conducting the leave-one-out cross-validation study so all of the testing and training data are comparable. Thus, our data are standardized climate anomalies that, for example, represent the number of standard deviations $P(\mathbf{s}, t)$ is above or below the time-averaged value $E_t[P(\mathbf{s}, t)]$ at location \mathbf{s} . The data are also spatially aggregated so that $n_s = 240$, 42 km-resolution grid cells cover Colorado and $n_r = 5, 252, 78$ km-resolution grid cells cover the Pacific Ocean. Distances between grid cells are measured with great-circle distances. We spatially aggregate the PRISM data to increase the smoothness of the data and to make the problem computationally tractable. We discuss alternate approaches to improve computational tractability in Section 4. The spatial aggregation and standardization also increase the normality of the data and provide a scale for precipitation with negative support, making it more appropriate for analysis with the RESP model’s Gaussian likelihood.

Pacific Ocean sea surface temperature capture how the ocean influences Colorado precipitation through the El Niño–Southern Oscillation (ENSO) teleconnection (Lukas, Barsugli, Doesken, Rangwala, & Wolter, 2014, Figure 2.4). The ENSO teleconnection is characterized

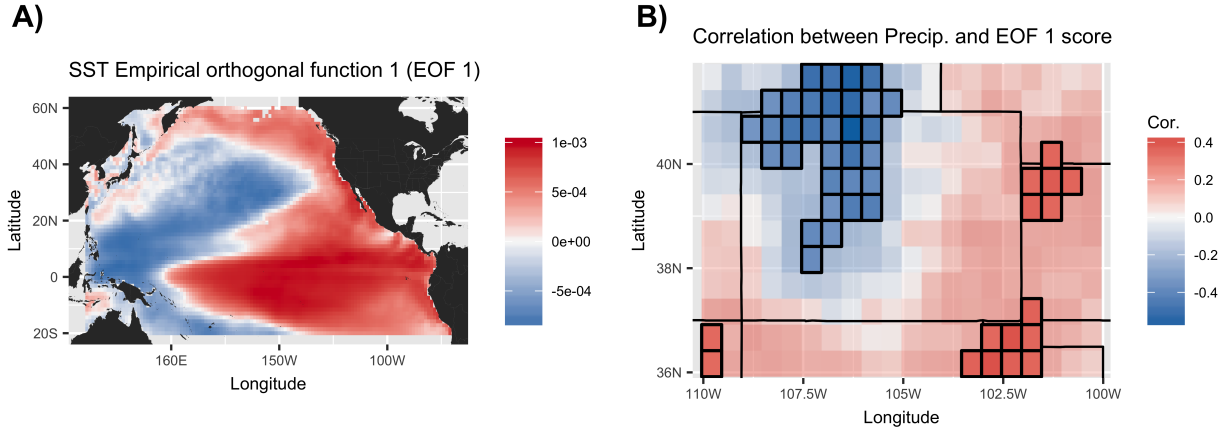


Figure 2: Exploratory analysis plots. A) The first empirical orthogonal function (EOF) $\psi_1 : \mathcal{D}_Y \rightarrow \mathbb{R}$ for standardized anomalies of Pacific Ocean sea surface temperatures is an indicator of El Niño events, during which sea surface temperatures are anomalously warm in the central and eastern Pacific Ocean tropics but anomalously cool in the western tropics (Ashok et al., 2007). EOF 1 accounts for 30% of the variability in sea surface temperatures. B) Pointwise correlations $\text{Cor}_t(P(\mathbf{s}, t), a_1(t))$ between Colorado precipitation $P(\mathbf{s}, t)$ and the EOF 1 score $a_1(t)$ suggest northern and western/central Colorado tends to receive less precipitation than average during El Niño events while eastern Colorado tends to receive more precipitation. Significant correlations (naive independent p-value $< .05$) are highlighted, while non-significant correlations are faded slightly.

by sea surface temperatures that are anomalously warm in the central and eastern Pacific Ocean tropics but anomalously cool in the western tropics. The first empirical orthogonal function (EOF; i.e., principal component) $\psi_1 : \mathcal{D}_Y \rightarrow \mathbb{R}$ for Pacific Ocean sea surface temperature anomalies illustrates this pattern (Figure 2). Pointwise correlations $\text{Cor}_t(a_1(t), P(\mathbf{s}, t))$ between the ENSO teleconnection’s strength $a_1(t)$ and Colorado precipitation $P(\mathbf{s}, t)$ provide standard evidence for teleconnection, suggesting northern and western/central Colorado tend to receive significantly less precipitation than average during ENSO events, which are periods of strong El Niño activity, while plains regions bordering eastern Colorado tend to receive significantly more precipitation than average (Figure 2).

3.2 RESP model and prior specification

In the RESP model (3), we specify a linear relationship between the local covariate T and response P so that β in (3) has intercept β_0 and slope β_T components $\beta = (\beta_0, \beta_T)^T$. While the RESP model as described in Section 2.1 uses a stationary covariance model and precipitation is non-stationary in space, stationary models have comparable predictive performance in Colorado (Paciorek & Schervish, 2006). For the RESP model’s remote coefficients, knots are placed at 93 locations that are roughly evenly spaced across the Pacific Ocean and along coastal locations (Supplement A, ??). While knot selection can be problematic, Banerjee et al. (2008) find that reasonably dense, regularly spaced grids can yield good results. Since the ENSO teleconnection is scientifically meaningful, we will interpret the transformed teleconnection effects $\alpha'(\mathbf{s}, 1)$ from (12), which are associated with ENSO through its connection to the first empirical orthogonal function (EOF) of sea surface temperature anomalies $\psi_1 : \mathcal{D}_Y \rightarrow \mathbb{R}$.

We adopt a combination of weakly informative and non-informative prior distributions. A dispersed normal prior is used for the fixed effects $\beta \sim \mathcal{N}(\mathbf{0}, 10I)$. We use $\sigma_w^2 \sim IG(2, 1)$, $\sigma_\varepsilon^2 \sim IG(2, 1)$, $\rho_w \sim U(1, 600)$, and $\rho_\alpha \sim U(1, 2000)$. The Matérn covariance smoothness parameters (7) are fixed at $\nu_w = \nu_\alpha = .5$, which correspond to the smoothest well-defined Matérn covariances for Gaussian processes on spheres (Gneiting, 2013). In exploratory analysis, variograms for the local and remote data fit this parameterization well. The prior for σ_α^2 is informative to increase the identifiability of this parameter and the remote range ρ_α (Zhang, 2004). The prior $\sigma_\alpha^2 \sim IG(6, 10)$ keeps the model from exploring parameter combinations that would imply very large teleconnection influence relative to the scale of the data $Y(\mathbf{s}, t)$.

3.3 Comparison models

We demonstrate the benefit of remote covariates by comparing the RESP model to RE and SP submodels that, respectively, exclude local and remote covariates. We also show improve-

ment to statistical downscaling and prediction by comparing RESP model validation scores to spatially varying coefficient (SVC) models (1) and other common downscaling models, including a hybrid local and non-local regression using the El-Niño–Southern Oscillation teleconnection (ENSO-T) (van den Dool, 2007, Sections 8.4, 8.5), canonical correlation analysis (CCA) (von Storch & Zwiers, 1999, Chapter 14), and a baseline climatological reference prediction (CLIM) (van den Dool, 2007, Section 8.1).

While analog models provide an alternate means to model teleconnected processes, we do not make comparisons to them in this application because analog models require more temporal replication than our data provide. Analog models require considerable temporal replication because predictions are weighted combinations of past observations, where the weights are based on distances between covariates at the prediction timepoint and all past observations (McDermott & Wikle, 2016). An advantage of analog forecasts, for example, is that the reweighting scheme naturally generates forecasts that have the same spatial patterns as past observations. Without enough past observations, however, the likelihood increases that past observations are not diverse enough to sufficiently approximate future states (Van Den Dool, 1994).

3.3.1 Spatially varying coefficient model (SVC)

To facilitate comparison, the SVC model (1) is specified with the same linear relationship between the local covariate T and response P we use with the RESP model. The scores $a_1(t)$ and $a_2(t)$ for the first and second sea surface temperature (SST) anomaly EOFs ψ_1 , ψ_2 capture ENSO and ENSO-Modoki teleconnection relationships for Colorado precipitation with bivariate spatially varying coefficients $\boldsymbol{\theta}(\mathbf{s}) \in \mathbb{R}^2$. The scores $\{a_i(t) : i = 1, 2, t \in \mathcal{T}\}$ quantify the strength of ENSO activity and are similar to other measures of ENSO activity (Ashok et al., 2007). The first and second EOFs ψ_1 and ψ_2 respectively account for 30% and 15% of the variability in SST.

We adopt a hierarchical Bayesian framework to estimate the SVC model (Banerjee et al.,

2015, Section 9.6.2). An Inverse-Wishart prior $\Lambda \sim IW(I, 2)$ is used for $\Lambda = \text{Cov}(\boldsymbol{\theta}(\mathbf{s}))$ and a dispersed normal prior is used for the fixed effects $\boldsymbol{\beta} \sim \mathcal{N}(\mathbf{0}, 10I)$. We use $\sigma^2 \sim IG(2, 1)$ and $\rho \sim U(1, 600)$ for the prior distribution of the Matérn covariance with fixed smoothness $\nu = .5$ for the model’s spatial correlation.

3.3.2 Hybrid local and non-local regression (ENSO-T)

Pointwise regression models are commonly used to downscale climate data (e.g., Towler et al., 2016). The ENSO-T model predicts precipitation $P(\mathbf{s}, t_0)$ at a location \mathbf{s} and new time point t_0 by applying a regression of training data $P(\mathbf{s}, t)$ onto local surface air temperature $T(\mathbf{s}, t)$ and the score $a_1(t)$ for the first sea surface temperature EOF $\psi_1 : \mathcal{D}_Y \rightarrow \mathbb{R}$. The ENSO-T downscaler provides a comparison model that accounts for both local and remote effects, but not spatial dependence.

3.3.3 Canonical correlation analysis (CCA)

Canonical correlation analysis uses the empirical correlation structure of sea surface temperature SST and precipitation P vectors to linearly map these variables to a space in which the transformed vectors are maximally correlated (von Storch & Zwiers, 1999, Chapter 14). This mapping may be used in a multivariate regression context with sea surface temperatures at new time points to predict precipitation. The mapping is often developed with some amount of smoothing by removing higher order EOFs from the data. We retain 16 EOFs in our use of CCA because this lets us capture approximately 90% of the variability in the predictors SST and predictand P . The CCA downscaler provides a comparison model that only accounts for remote effects and indirectly accounts for spatial dependence.

3.3.4 Climatological reference (CLIM)

Climatologists use the unconditional distribution of precipitation $P(\mathbf{s}, t)$ at a location \mathbf{s} . When no other information is available, the average value of precipitation $E_t[P(\mathbf{s}, t)]$ is

used as a climatological point prediction for precipitation, and the empirical distribution is used for probabilistic predictions. The CLIM downscaler provides a baseline comparison model that does not account for spatial dependence, local, or remote effects.

3.4 Results

Model results are based on 20,000 samples from the posterior distribution after a burn in period of 1,000 samples. Convergence was assessed by examining trace plots, autocorrelation plots, and effective sample sizes in addition to comparing results from multiple runs with randomly initialized parameters. Model adequacy was assessed using residual and qq-normal plots. These diagnostics suggest there are no serious violations of the convergence and distributional assumptions. Variance inflation factors (VIFs) that account for the RESP model design also show no concern for multicollinearity in the fitted model ??.

3.4.1 Inference

Parameter estimates for the RESP model yield reasonable scientific interpretations (Table 1). The sign of the regression coefficient β_T for the temperature covariate T is consistent with physical processes that influence precipitation (Daly et al., 2008). The local covariance range parameter ρ_w implies the dependence between locations $\mathbf{s} \in \mathcal{D}_Y$ has an effective range between 500 and 570 km, which is the distance between locations beyond which the Matérn correlation (7) is small ($\leq .05$). This length scale is in the size range of mesoscale weather processes that produce precipitation (Parker, 2015). The remote covariance range parameter ρ_α implies the dependence between locations $\mathbf{r} \in \mathcal{D}_Z$ has an effective range between 720 and 2,200 km, which is roughly the size of the mid-sized structures seen in the EOF patterns in Figure 2 A. Since local temperature T is teleconnected with sea surface temperatures SST , remote effects must be interpreted as residual teleconnection effects, as described at the end of Section 2.4. Significant remote effects suggest Colorado’s teleconnection with the Pacific Ocean cannot be represented through a linear relationship with temperature alone; the

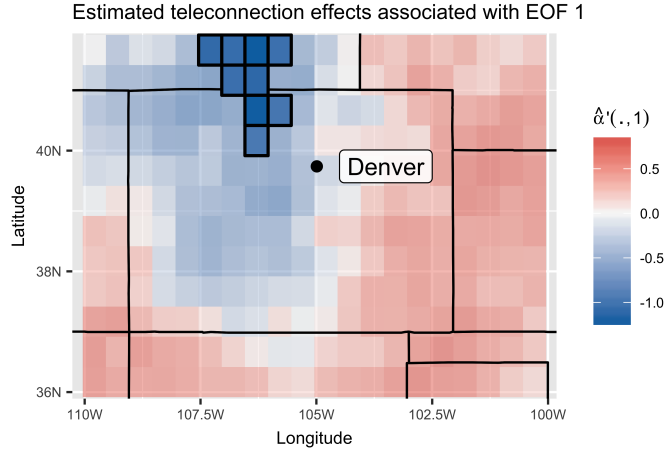


Figure 3: Estimated teleconnection effects $\hat{\alpha}'(\mathbf{s}, 1)$ for EOF 1 $\psi_1 : \mathcal{D}_Y \rightarrow \mathbb{R}$. The overall patterns yield similar interpretations as those made with the Figure 2 exploratory plots, however, the RESP model reduces the regions in which evidence exists for significant teleconnection. Significant teleconnection effects, as determined using 95% highest posterior density intervals, are highlighted.

teleconnection likely involves non-linear relationships and additional variables or interactions. Posterior estimates for the transformed remote effects $\{\alpha'(\mathbf{s}, 1) : \mathbf{s} \in \mathcal{D}_Y\}$ associated with $\psi_1 : \mathcal{D}_Y \rightarrow \mathbb{R}$ (Figure 3) largely match the exploratory pointwise correlations between $P(\mathbf{s}, t)$ and $a_1(t)$ found in the exploratory plot (Figure 2), indicating the RESP model (3) is capturing known Colorado teleconnections. Fewer locations have significant teleconnection, however, as the estimates incorporate more uncertainty due to spatial correlation; significance is determined with respect to evaluating highest posterior density intervals, separately for each location $\mathbf{s} \in \mathcal{D}_Y$.

3.4.2 Model validation

Leave-one-out cross-validation scores demonstrate the RESP model benefits from including remote covariates and offers improvement over comparison models in the intended prediction-like setting of perfect prognosis downscaling (Figure 4). The RESP and comparison models are trained on all but one year of available data, then used to predict the responses

$\{P(\mathbf{s}, t) : \mathbf{s} \in \mathcal{D}_Y\}$ for the test year t to mimic the perfect prognosis downscaling setting in which a climate variable must be completely inferred from covariate data only. The process is repeated with all years of available data. While the RESP and comparison models yield continuous predictive distributions, we discretize the distributions before assessing them. Climate forecasts are often discretized because it is inherently difficult to develop more precise climate predictions at seasonal and longer time scales (Mason, 2012; van den Dool, 2007, Section 9.6). We use the empirical terciles $\hat{q}(1/3; P(\mathbf{s}, \cdot))$ and $\hat{q}(2/3; P(\mathbf{s}, \cdot))$ to discretize the predictive distribution $f(P(\mathbf{s}, t_0) | \mathbf{P})$ at each location $\mathbf{s} \in \mathcal{D}_Y$ into “below average”, “near average”, and “above average” categories. While it is possible to directly fit discrete models to the data, doing so is not necessarily helpful. For example, a probit-link RESP or SVC model would require re-estimation of observed continuous data $P(\mathbf{s}, t)$ as latent fields (Higgs & Hoeting, 2010).

We use ranked probability scores (RPS) to assess probabilistic forecasts for ordinal variables, giving lower scores to models that generate predictive distributions that better match the true distribution (Gneiting & Raftery, 2007). The CCA model only yields point predictions since predictive uncertainties are difficult to obtain. Thus, the CCA’s validation scores are inflated since its discretized predictive distribution is defined by a point mass on the category that matches the tercile in which the point prediction lies.

The RESP model (3) frequently yields better probabilistic predictions than the comparison models. In particular, the RESP model performs better than the RE or SP submodels which highlights the advantage of combining local and remote information. Sample maps of predictions and uncertainties are presented in Supplement A ???. The RESP model also tends to perform better than the SVC model which highlights the advantage of not specifying teleconnection indices a priori and adding additional spatial structure to estimates of teleconnection effects. Similar results are obtained using Heidke skill scores to compare models. Heidke skill scores are commonly used in climate science to measure a model’s misclassification rate for categorical point predictions (von Storch & Zwiers, 1999, Section

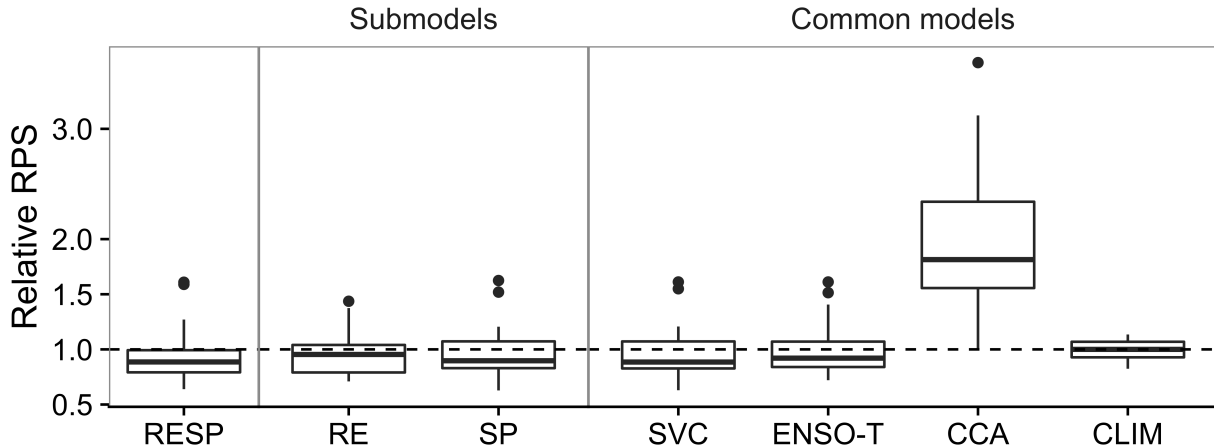


Figure 4: Comparison of Ranked probability scores (RPS) for probabilistic categorical predictions on the leave-one-out test datasets for the RESP and comparison models. RPS scores are reported relative to the median RPS for the CLIM reference model’s unconditional predictions. The RESP model generally has better (i.e., lower) and slightly less variable skill than the “Sub” and “Common” comparison models.

18.1). Formulas and details for RPS and Heidke skill scores can be found in Supplement A ??.

4 Discussion

The RESP model (3) expands geostatistical frameworks that incorporate the effect of both local and remote covariates on spatially correlated responses, like precipitation, but can be extended to address additional spatio-temporal modeling needs. For example, while we use the RESP model to draw inference on entire response fields, the model’s process-formulation also allows it to be applied to more standard spatial interpolation problems as well. Since there is great uncertainty in global climate model (GCM) predictions of future precipitation, statistical downscaling methods have been widely used in regional climate change studies. Validating the RESP model on historical data marks an improvement on existing approaches

and implies it can be used with GCM predictions of surface temperatures and large-scale patterns to infer predictions for precipitation from covariate data only. By comparison with the RESP model, other models directly model less of the spatial structure in teleconnected data, but other models have been studied in broader statistical contexts. Fortunately, it is possible to formulate the RESP model more broadly.

Many scientific disciplines work with spatially-referenced non-Gaussian data, for which the RESP model can be adapted. For example, the RESP model could be adapted to study teleconnective effects on the number of large rain events, which are important for many ecological systems and sectors of society. Following approaches common to generalized linear models for spatial data, the existing RESP response $Y(\mathbf{s}, t)$ may be reinterpreted as a latent Gaussian field that helps parameterize the distribution for non-Gaussian observations (Diggle, Tawn, & Moyeed, 1998; Higgs & Hoeting, 2010). The primary technical challenge for Bayesian implementations of such models is to develop efficient estimation procedures since conjugacy is lost.

Modeling effects for multivariate remote covariates or data on large spatial domains could both be facilitated by modeling spatial dependence with sparse geostatistical models. Inference and prediction for many geostatistical models involves matrix operations with $O(n_s^3)$ computational complexity. Sparse geostatistical models can avoid these costs on large spatial domains, for example, by using Gaussian Markov random field approximations to specific classes of Gaussian fields with Matérn covariances (Lindgren et al., 2011), covariance tapering to generate spatial covariance matrices with banded structure (Furrer, Genton, & Nychka, 2006), multiresolution covariance models (Katzfuss, 2016), or hierarchical nearest neighbor models (Datta, Banerjee, Finley, & Gelfand, 2016). While computational savings may be minimal for small spatial domains like Colorado, they may offset computational costs of estimating teleconnection effects for multiple sets of remote covariates. The RESP model may naturally be extended to include multiple teleconnection effects (4) to model impacts from Pacific and Atlantic Ocean temperatures, for example. Multivariate telecon-

nection effects can also be used to model impacts from a vector $\mathbf{z}(\mathbf{r}, t) \in \mathbb{R}^m$ of m remote covariates at location $\mathbf{r} \in \mathcal{D}_Z$. Both extensions require sensibly modifying the remote coefficient covariance function (6) and will yield likelihood structures similar to the RESP model (3), especially if relationships between additional teleconnection effects are modeled with separable covariances.

Non-stationary covariance models and temporal extensions can also allow the RESP model to be applied to more diverse data and problems. While the teleconnection term (4) admits temporal non-stationarity moderated by the remote covariates, modeling temporal dependence across timepoints can allow the RESP model to be used in more traditional forecasting problems. Similarly, modeling spatial non-stationarity can potentially improve model fit and prediction at unobserved spatial locations. In particular, nonstationary covariances could allow the remote coefficients to vary temporally. This extension may be relevant because Mason and Goddard (2001) find that teleconnection effects can vary across seasons. As in Choi et al. (2015), however, changes over time may be difficult to detect because the effects tend to be weak.

Without considering any extensions, however, the RESP model yields additional discussion about spatial modeling. The RESP model’s inclusion of dependence at both long and short distances echoes descriptions of the screening effect (Stein, 2015). Carefully studying spectral densities of covariance functions show that if they decay quickly enough, then spatial predictions are primarily driven by data from nearby locations. While the RESP model allows distant locations to influence spatial prediction, the RESP model does not contradict the screening effect because it explicitly models long range dependence through the teleconnection term (4) and the screening effect is a property of local covariance functions (5). Of similar subtlety, maps of estimated teleconnection effects (Figure 3) raise discussion about uncertainty estimates for spatial patterns. Significance in Figure 3 is determined pointwise with respect to the posterior distribution for $\alpha'(\mathbf{s}, 1)$ at each location so can provide inference for teleconnection effects at individual points. Here, pointwise significance can help

individual municipalities determine whether they are strongly impacted by teleconnection effects and may benefit from use of the RESP model. Determining uncertainty for entire regions is a multiple testing problem not considered in this study (Bolin & Lindgren, 2015; French & Hoeting, 2016). Uncertainties for entire regions are more important, for example, when trying to estimate boundaries for polluted areas.

There is potential for more diverse application of the RESP model because teleconnections exist in other fields, like ecology (Brierley, Demer, Watkins, & Hewitt, 1999) and human geography (Seto et al., 2012). The model's general introduction in Section 2 as a spatial regression problem highlights a less-common class of spatial analysis problems because it addresses problems that require dependence at both long and short distances, at odds with typical assumptions that data at distant points are effectively independent. While the RESP model assumes the response and remote covariates are defined on disjoint spatial domains, it suggests even broader classes of problems in which overlapping domains characterize dependence between distant locations, or in which teleconnected domains are not known a priori and need to be estimated. The latter problem is reminiscent of general covariance or graphical model structure estimation problems, which may provide possible directions for future spatial statistics research topics.

Supplementary materials

Additional information and supporting material for this article is available online at the journal's website.

Acknowledgements

We express our gratitude to Michael Stein and Mikael Kuusela for discussions that helped enrich interpretations of the RESP model. This material is based upon work supported by the National Science Foundation under grant numbers AGS-1419558 and DMS-1106862. Any

opinions, findings, and conclusions or recommendations expressed in this material are those of the authors and do not necessarily reflect the views of the National Science Foundation.

References

- Adler, R. J., & Taylor, J. E. (2007). *Random Fields and Geometry*. New York: Springer Science + Business Media, LLC.
- Ashok, K., Behera, S. K., Rao, S. A., Weng, H., & Yamagata, T. (2007). El Nino Modoki and its possible teleconnection. *Journal of Geophysical Research*, *112*, 1–27.
- Assunção, R., & Krainski, E. (2009). Neighborhood Dependence in Bayesian Spatial Models. *Biometrical Journal*, *51*(5), 851–869.
- Banerjee, S., Carlin, B. P., & Gelfand, A. E. (2015). *Hierarchical Modeling and Analysis for Spatial Data* (Second ed.). Boca Raton, FL: CRC Press.
- Banerjee, S., Gelfand, A. E., Finley, A. O., & Sang, H. (2008). Gaussian predictive process models for large spatial data sets. *Journal of the Royal Statistical Society. Series B: Statistical Methodology*, *70*(4), 825–848.
- Bolin, D., & Lindgren, F. (2015). Excursion and contour uncertainty regions for latent Gaussian models. *Journal of the Royal Statistical Society: Series B (Statistical Methodology)*, *77*, 85–106.
- Brierley, A. S., Demer, D. A., Watkins, J. L., & Hewitt, R. P. (1999). Concordance of interannual fluctuations in acoustically estimated densities of Antarctic krill around South Georgia and Elephant Island: Biological evidence of same-year teleconnections across the Scotia Sea. *Marine Biology*, *134*, 675–681.
- Bruyere, C. L., Holland, G. J., & Towler, E. (2012). Investigating the Use of a Genesis Potential Index for Tropical Cyclones in the North Atlantic Basin. *Journal of Climate*, *25*, 8611–8626.
- Calder, C. A., Craigmire, P. F., & Mosley-Thompson, E. (2008). Spatial variation in the

- influence of the North Atlantic Oscillation on precipitation across Greenland. *Journal of Geophysical Research*, 113.
- Choi, I., Li, B., Zhang, H., & Li, Y. (2015). Modelling space-time varying ENSO teleconnections to droughts in North America. *Stat*, 4(1), 140–156.
- Daly, C., Halbleib, M., Smith, J. I., Gibson, W. P., Doggett, M. K., Taylor, G. H., . . . Pasteris, P. P. (2008). Physiographically sensitive mapping of climatological temperature and precipitation across the conterminous United States. *International Journal of Climatology*, 28(15), 2031–2064.
- Datta, A., Banerjee, S., Finley, A., & Gelfand, A. (2016). Hierarchical Nearest-Neighbor Gaussian Process Models for Large Geostatistical Datasets. *Journal of the American Statistical Association*, 111(514), 800–812.
- Dee, D. P., Uppala, S. M., Simmons, A. J., Berrisford, P., Poli, P., Kobayashi, S., . . . Vitart, F. (2011). The ERA-Interim reanalysis: Configuration and performance of the data assimilation system. *Quarterly Journal of the Royal Meteorological Society*, 137(656), 553–597.
- Deser, C., Phillips, A., Bourdette, V., & Teng, H. (2012). Uncertainty in climate change projections : the role of internal variability. *Climate Dynamics*, 38, 527–546.
- Diggle, P. J., Tawn, J. A., & Moyeed, R. A. (1998). Model-Based Geostatistics. *Journal of the Royal Statistical Society, Series C*, 47(3), 299–350.
- Dong, B., & Dai, A. (2015). The influence of the Interdecadal Pacific Oscillation on Temperature and Precipitation over the Globe. *Climate Dynamics*, 45, 2667–2681.
- Flato, G., Marotzke, J., Abiodun, B., Braconnot, P., Chan Chou, S., Collins, W., . . . Rummukainen, M. (2013). Evaluation of Climate Models 9. In *Climate change 2013: The physical science basis. contribution of working group i to the fifth assessment report of the intergovernmental panel on climate change* (pp. 741–882). Cambridge, United Kingdom: Cambridge University Press.
- Fowler, H. J., Blenkinsop, S., & Tebaldi, C. (2007). Linking climate change modelling to

- impacts studies : recent advances in downscaling techniques for hydrological. *International Journal of Climatology*, *27*, 1547–1578.
- French, J. P., & Hoeting, J. A. (2016). Credible regions for exceedance sets of geostatistical data. *Environmetrics*, *27*, 4–14.
- Furrer, R., Genton, M. G., & Nychka, D. (2006). Covariance Tapering for Interpolation of Large Spatial Datasets. *Journal of Computational and Graphical Statistics*, *15*(3), 502–523.
- Gneiting, T. (2013). Strictly and non-strictly positive definite functions on spheres. *Bernoulli*, *19*(4), 1327–1349.
- Gneiting, T., & Raftery, A. E. (2007). Strictly Proper Scoring Rules, Prediction, and Estimation. *Journal of the American Statistical Association*, *102*(477), 359–378.
- Goddard, L., Mason, S. J., Zebiak, S. E., Ropelewski, C. F., Basher, R., & Cane, M. A. (2001). Current approaches to seasonal-to-interannual climate predictions. *International Journal of Climatology*, *21*, 1111–1152.
- Higgs, M. D., & Hoeting, J. A. (2010). A clipped latent variable model for spatially correlated ordered categorical data. *Computational Statistics and Data Analysis*, *54*(8), 1999–2011.
- Karl, T. R., Wang, W.-C., Schlesinger, M. E., Knight, R. W., & Portman, D. (1990). A Method of Relating General Circulation Model Simulated Climate to the Observed Local Climate. Part I: Seasonal Statistics. *Journal of Climate*, *3*, 1053–1079.
- Katzfuss, M. (2016). A multi-resolution approximation for massive spatial datasets. *Journal of the American Statistical Association*, *112*(517), 201–214.
- Lindgren, F., Rue, H., & Lindström, J. (2011). An explicit link between gaussian fields and gaussian markov random fields: The stochastic partial differential equation approach. *Journal of the Royal Statistical Society. Series B: Statistical Methodology*, *73*(4), 423–498.
- Lukas, J., Barsugli, J., Doesken, N., Rangwala, I., & Wolter, K. (2014). *Climate Change in*

- Colorado* (Second ed.). University of Colorado Boulder.
- Mantua, N. J., Hare, S. R., Zhang, Y., Wallace, J. M., & Francis, R. C. (1997). A Pacific Interdecadal Climate Oscillation with Impacts on Salmon Production. *Bulletin of the American Meteorological Society*, *78*(6), 1069–1079.
- Maraun, D., Wetterhall, F., Chandler, R. E., Kendon, E. J., Widmann, M., Brienen, S., ... Thiele-Eich, I. (2010). Precipitation downscaling under climate change: Recent developments to bridge the gap between dynamical models and the end user. *Reviews of Geophysics*, *48*(RG3003).
- Mason, S. J. (2012). Seasonal and longer-range forecasts. In I. T. Jolliffe & D. B. Stephenson (Eds.), *Forecast verification: A practitioner's guide in atmospheric science* (Second ed., pp. 204–220). Oxford: John Wiley & Sons, Ltd.
- Mason, S. J., & Goddard, L. (2001). Probabilistic precipitation anomalies associated with ENSO. *Bulletin of the American Meteorological Society*, *82*, 619–638.
- McDermott, P. L., & Wikle, C. K. (2016). A model-based approach for analog spatio-temporal dynamic forecasting. *Environmetrics*, *27*, 70–82.
- Meehl, G. A., Goddard, L., Boer, G., Burgman, R., Branstator, G., Cassou, C., ... Yeager, S. (2014). Decadal climate prediction: An update from the trenches. *Bulletin of the American Meteorological Society*, *95*(2), 243–267.
- Meehl, G. A., Goddard, L., Murphy, J., Stouffer, R. J., Boer, G., Danabasoglu, G., ... Stockdale, T. (2009, oct). Decadal Prediction. *Bulletin of the American Meteorological Society*, *90*(10), 1467–1485.
- Montroy, D. (1997). Linear Relation of Central and Eastern North American Precipitation to Tropical Pacific Sea Surface Temperature Anomalies. *Journal of Climate*, *10*, 541–558.
- Montroy, D., Richman, M. B., & Lamb, P. J. (1998). Observed Nonlinearities of Monthly Teleconnections between Tropical Pacific Sea Surface Temperature Anomalies and Central and Eastern North American Precipitation. *Journal of Climate*, *11*, 1812–1835.
- Nigam, S., & Baxter, S. (2015). Teleconnections. In *Encyclopedia of atmospheric sciences*

- 2nd edition* (Second ed., Vol. 3, pp. 90–109). Elsevier Ltd.
- Paciorek, C. J., & Schervish, M. J. (2006). Spatial modelling using a new class of nonstationary covariance functions. *Environmetrics*, *17*(5), 483–506.
- Parker, D. (2015). Mesoscale Meteorology. In *Encyclopedia of atmospheric sciences 2nd edition* (Vol. 3, pp. 316–322). Elsevier Ltd.
- Seto, K. C., Reenberg, A., Boone, C. G., Fragkias, M., Haase, D., Langanke, T., . . . Simon, D. (2012). Urban land teleconnections and sustainability. *Proceedings of the National Academy of Sciences*, *109*(20), 7687–7692.
- Stein, M. L. (2015). When does the screening effect not hold? *Spatial Statistics*, *11*, 65–80.
- Ting, M. F., & Wang, H. (1997). Summertime U.S. precipitation variability and its Relation to Pacific Sea Surface Temperature. *Journal of Climate*, *10*(8), 1853–1873.
- Towler, E., PaiMazumder, D., & Holland, G. (2016). A framework for investigating large-scale patterns as an alternative to precipitation for downscaling to local drought. *Climate Dynamics*, 1–12.
- Tsonis, A. A., & Swanson, K. L. (2008). On the Role of Atmospheric Teleconnections in Climate. *Journal of Climate*, *21*, 2990–3001.
- Van Den Dool, H. M. (1994). Searching for analogues, how long must we wait? *Tellus*, *46A*(314-324).
- van den Dool, H. (2007). *Empirical Methods in Short-Term Climate Predictions*. Oxford: Oxford University Press.
- von Storch, H., & Zwiers, F. W. (1999). *Statistical Analysis in Climate Research*. Cambridge: Cambridge University Press.
- Wall, M. M. (2004). A close look at the spatial structure implied by the CAR and SAR models. *Journal of Statistical Planning and Inference*, *121*, 311–324.
- Ward, P. J., Jongman, B., Kummu, M., Dettinger, M. D., Sperna Weiland, F. C., & Winsemius, H. C. (2014). Strong influence of El Nino Southern Oscillation on flood risk

around the world. *Proceedings of the National Academy of Sciences*, 111(44), 15659–15664.

Wikle, C. K., & Anderson, C. J. (2003). Climatological analysis of tornado report counts using a hierarchical Bayesian spatiotemporal model. *Journal of Geophysical Research*, 108(D24).

Wilby, R. L., Wigley, T. M. L., Conway, D., Jones, P. D., Hewitson, B. C., Main, J., & Wilks, D. S. (1998). Statistical downscaling of general circulation model output : A comparison of methods. *Water Resources Research*, 34(11), 2995–3008.

Zhang, H. (2004). Inconsistent Estimation and Asymptotically Equal Interpolations in Model-Based Geostatistics. *Journal of the American Statistical Association*, 99(465), 250–261.

Table 1: Posterior mean estimates and 95% highest posterior density (HPD) intervals for the RESP model’s parameters, which include an intercept β_0 and temperature effect β_T on the mean response (see equation (3)), and covariance scale σ^2 and range ρ parameters for the local w and remote α spatial dependence and nugget effect ε (see (5) and (6)). The smoothness parameters ν_w and ν_α were fixed (Section 3.2).

		Posterior mean	95% HPD
Local effects	β_0	-0.00	(-0.14, 0.14)
	β_T	-0.18	(-0.24, -0.12)
Covariance	σ_w^2	0.55	(0.49, 0.62)
	σ_α^2	6.05	(1.04, 14.81)
	σ_ε^2	0.01	(0.01, 0.01)
	ρ_w	248.00	(220, 280)
	ρ_α	509.00	(266, 799)